Electronic and magnetic structures of the postperovskite-type Fe_2O_3 and implications for planetary magnetic records and deep interiors

Sang-Heon Shim[a,1], Amelia Bengtson[b], Dane Morgan[b], Wolfgang Sturhahn[c], Krystle Catalli[a], Jiyong Zhao[c], Michael Lerche[c,d], and Vitali Prakapenka[e]

[a]Department of Earth, Atmospheric, and Planetary Science, Massachusetts Institute of Technology, 77 Massachusetts Avenue, Cambridge, MA 02139; [b]Department of Materials Science and Engineering, University of Wisconsin, 1509 University Avenue, Madison, WI 53706; [c]X-ray Science Division, Argonne National Laboratory, 9700 South Cass Avenue, Argonne, IL 60439; [d]High Pressure Synergetic Center, Carnegie Institution of Washington, 9700 South Cass Avenue, Argonne, IL 60439; and [e]Center for Advanced Radiation Sources, University of Chicago, 5640 South Ellis Avenue, Chicago, IL 60637

Edited by Russell J. Hemley, Carnegie Institution of Washington, Washington, DC, and approved February 3, 2009 (received for review August 28, 2008)

Recent studies have shown that high pressure (*P*) induces the metallization of the Fe^{2+}–O bonding, the destruction of magnetic ordering in Fe, and the high-spin (HS) to low-spin (LS) transition of Fe in silicate and oxide phases at the deep planetary interiors. Hematite (Fe_2O_3) is an important magnetic carrier mineral for deciphering planetary magnetism and a proxy for Fe in the planetary interiors. Here, we present synchrotron Mössbauer spectroscopy and X-ray diffraction combined with ab initio calculations for Fe_2O_3 revealing the destruction of magnetic ordering at the hematite → Rh_2O_3-II type (RhII) transition at 70 GPa and 300 K, and then the revival of magnetic ordering at the RhII → postperovskite (PPv) transition after laser heating at 73 GPa. At the latter transition, at least half of Fe^{3+} ions transform from LS to HS and Fe_2O_3 changes from a semiconductor to a metal. This result demonstrates that some magnetic carrier minerals may experience a complex sequence of magnetic ordering changes during impact rather than a monotonic demagnetization. Also local Fe enrichment at Earth's core-mantle boundary will lead to changes in the electronic structure and spin state of Fe in silicate PPv. If the ultra-low-velocity zones are composed of Fe-enriched silicate PPv and/or the basaltic materials are accumulated at the lowermost mantle, high electrical conductivity of these regions will play an important role for the electromagnetic coupling between the mantle and the core.

spin ordering | electrical conductivity | high pressure | phase transition

The origin of the magnetism in hematite (Fe_2O_3) has long drawn interest. It is a ubiquitous mineral on the oxidizing surfaces of the terrestrial planets, such as Earth and Mars, and is an important magnetic carrier mineral for deciphering the magnetic history of the planets. Furthermore, it serves as a proxy for the phases in the Earth's core and mantle, as oxygen may be an important alloying elements in the core and as Fe enters the dominant silicate and oxide phases in the mantle. Fe_2O_3 has a stability field for the postperovskite (PPv) - type crystal structure (1) to which the dominant lower mantle silicate transforms at the pressure (*P*)–temperature (*T*) conditions corresponding to the D″ region (bottom 200- to 400-km-depth region of the mantle) (2–4).

A previous study (5) showed a large increase in electrical conductivity in FeO at mantle related *P*, suggesting that the Fe^{2+}–O bonding character changes from covalent/ionic to metallic. An ab initio study (6) predicted a magnetic collapse of Fe in silicates and oxides at high *P*, perhaps within the deep mantle. A high-spin (HS) → low-spin (LS) transition has been observed in silicates and oxides at mantle related *P* (7–9). These transitions can induce changes in important properties, such as elasticity, optical properties, electrical conductivity, and element partitioning (7, 10, 11). Recent ab initio studies suggested that structure and composition can have enormous influence on the spin transition, e.g., yielding large and opposite trends in transition pressure with composition for perovskite (Pv) and ferropericlase (Fp) (12, 13). Therefore, it is important to investigate how these electronic and magnetic transitions will be influenced by structural transitions and compositional variations existing in the deep Earth's interior.

Some iron oxides and sulfides carry important paleomagnetic records. However, impacts can disturb or even erase the records. For example, magnetic fields can be generated during a shock event, providing a possible explanation for high magnetic remanence found in young lunar glasses (14). In addition, a recent study suggested that randomization of paleomagnetic records by impact-generated fields may be responsible for the weak magnetic field intensity observed at the impact basins of Mars (15). As shown for pyrrhotite (16), impacts can demagnetize minerals, providing an alternative interpretation for the weak fields at the impact basins. Yet, high-*P* behaviors of most magnetic carrier minerals are not well studied.

Several intriguing changes have been observed in Fe_2O_3 at $40 \leq P \leq 60$ GPa: a large increase in density (14%) and a drastic drop in resistivity (17–19), a phase transition to a Rh_2O_3-II (RhII) type structure (20), disappearance of magnetic hyperfine fields during the hematite → RhII transition (19), and the HS → LS transition of Fe (21).

Although Fe end member is stable in the MgO–FeO system that forms the second most abundant mantle phase, it is not stable and therefore not accessible experimentally for PPv in the $MgSiO_3$–$FeSiO_3$ system that forms the most abundant phase in the D″ region. It has recently been found that the PPv phase is stable at 2,000 K and 60 GPa with an Fe_2O_3 stoichiometry (1). Furthermore, some studies suggested that a substantial amount of Fe in Mg-silicate Pv and PPv are Fe^{3+} ($Fe^{3+}/\sum Fe = 0.1 \sim 0.7$) at mantle *P*–*T* conditions due to crystal chemistry effects (22, 23). Therefore, Fe_2O_3 provides opportunities to understand the properties of Fe end-member PPv.

Here, we report the synchrotron Mössbauer spectroscopy (SMS) and X-ray diffraction (XRD) of Fe_2O_3-PPv as well as the other Fe_2O_3 polymorphs at high *P*. We find that Fe in both the octahedral (hereafter B) and bipolar-prismatic (hereafter A) sites are magnetically ordered and, combined with our ab initio calculations, Fe in at least one of the two sites is in a HS state in PPv. Therefore, Fe_2O_3 undergoes a series of transitions: magnetic insulator with HS Fe^{3+} → nonmagnetic semiconductor with LS Fe^{3+} → magnetic metal with at least half of Fe^{3+} in HS, during

Author contributions: S.-H.S. designed research; S.-H.S., A.B., D.M., and K.C. performed research; W.S., J.Z., M.L., and V.P. contributed new reagents/analytic tools; S.-H.S., A.B., D.M., and W.S. analyzed data; and S.-H.S., A.B., and D.M. wrote the paper.

The authors declare no conflict of interest.

This article is a PNAS Direct Submission.

[1]To whom correspondence should be addressed. E-mail: sangshim@mit.edu.

This article contains supporting information online at www.pnas.org/cgi/content/full/0808549106/DCSupplemental.

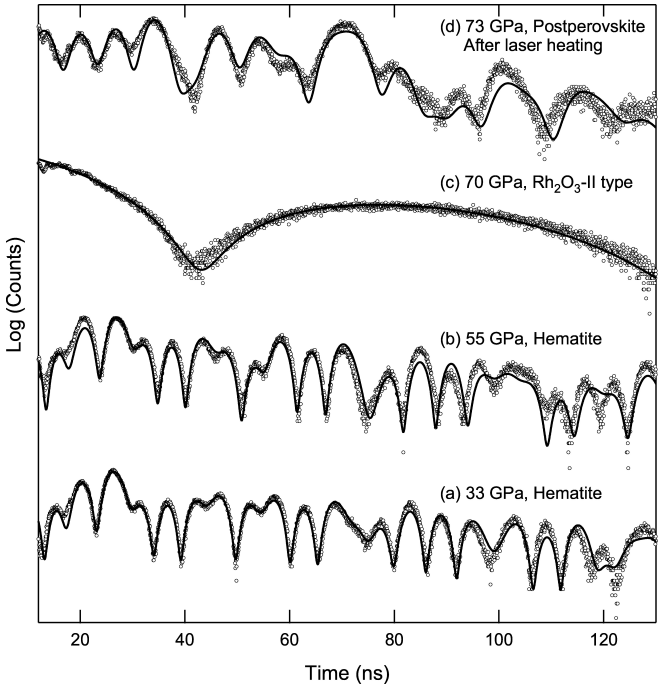

Fig. 1. SMS of Fe_2O_3 polymorphs at high *P*. The open circles and thick curves represent observed and fitted spectra, respectively.

hematite → RhII type → PPv transitions, suggesting strong influence of crystal structure on the electronic and magnetic structures of Fe.

Results and Discussions

The Morin transition in Fe_2O_3, where canted antiferromagnetic (AFM) → AFM, results in a large change in quadrupole splitting ($QS = 0.4 \rightarrow -0.8$ mm/s) at 1.5 GPa (24). Our *QS* and magnetic hyperfine field (B_{hf}) obtained from the spectral fitting of SMS between 33 and 55 GPa (Fig. 1*A* and *B*) are in complete agreement with conventional Mössbauer results of the AFM phase (19, 25) and these values change only slightly with *P* (Table 1), indicating that Fe_2O_3 remains AFM to 55 GPa. Our XRD shows that the sample remains in the hematite phase up to 55 GPa at 300 K.

At 70 GPa and 300 K, our XRD confirms a complete transformation to the RhII phase, consistent with previous studies (20). We found a very simple Mössbauer spectrum for the RhII phase (Fig. 1*C*). The time spectra obtained from Nuclear Forward Scattering can be regarded as modulated decay curves resulting from the energy differences in the nuclear transitions, i.e., the nuclear energy level splitting. In general, the absence of a magnetic hyperfine field results in much less modulation in the time spectra for a reasonable *QS* range. Indeed, the best spectral fitting was achieved with a single Fe site with $QS = 0.84 \pm 0.01$ mm/s but without magnetic hyperfine field. This indicates that the magnetic ordering is destroyed at 70 GPa, which is in agreement with a conventional Mössbauer result (19). Also, the single-site model is consistent with the RhII type structure.

After observing the transition to the RhII phase, we conducted laser heating of the sample up to 2,000 K at 70 GPa for 30 min. After heating, the sample is completely transformed to another orthorhombic phase (Fig. 2), the diffraction pattern of which fits well to the PPv type. The fitted unit-cell parameters are also consistent with a previous report within 0.6% (1). We also conducted in situ high *P*–*T* diffraction by using a separate sample. Before heating, diffraction patterns indicate that the sample has transformed to the RhII phase (Fig. 2*A*). During heating the most intense line of PPv appears at 1,250 K. After 10 min of heating at 1,500 K, we observed strong growth of PPv. To transform the sample completely to PPv, we heated to 2,000 K (Fig. 2*C*). Pure PPv remains after *T* quench (Fig. 2*D*). In the second heating cycle at 70 GPa, we heat Fe_2O_3-PPv to a low *T*, 1,200 K, for 30 min. We did not observe any sign of a reverse transformation to the RhII phase, indicating that the PPv phase is thermodynamically stable at 70 GPa.

The SMS of Fe_2O_3-PPv shows much more modulation than that of the RhII phase, but less than that of hematite (Fig. 1), strongly suggesting finite magnetic moments for Fe^{3+} in PPv. The best spectral fitting is achieved when we include two different Fe sites both with finite B_{hf} and *QS*. The Fe occupancy ratio between the two sites is found to be 6:4 (Table 1). Considering the fact that we assumed the same Mössbauer responses, such as recoil-free fractions, from the different Fe sites (26), the result can be regarded as a reasonable agreement with the proposed crystal structure of PPv (1, 2, 27) which has two different cation sites, octahedral and bipolar prismatic, with a 1:1 molar ratio.

The finite B_{hf} for the two different sites clearly indicates that Fe_2O_3-PPv is magnetic. To understand the magnetic ordering and

Table 1. Fitted Mössbauer parameters of Fe_2O_3 at high pressures

Pressure, GPa		*QS*, mm/s	B_{hf}, T	ΔIS, mm/s	Site occupancy
			Hematite		
33(2)		−0.93(1)	51.11(2)		
47(3)		−1.09(2)	50.23(3)		
55(3)		−1.15(1)	49.86(3)		
			Rh_2O_3-II type		
70(4)		0.84(1)			
			Postperovskite type		
73(4)	Site 1	0.48(4)	39.73(6)	0.30(2)	0.6(1)
	Site 2	−0.31(7)	19.21(11)		0.4

Numbers in parentheses are 2σ uncertainties (*QS*, quadrupole splitting; B_{hf}, magnetic hyperfine field; ΔIS, isomer shift difference between the two different Fe sites).

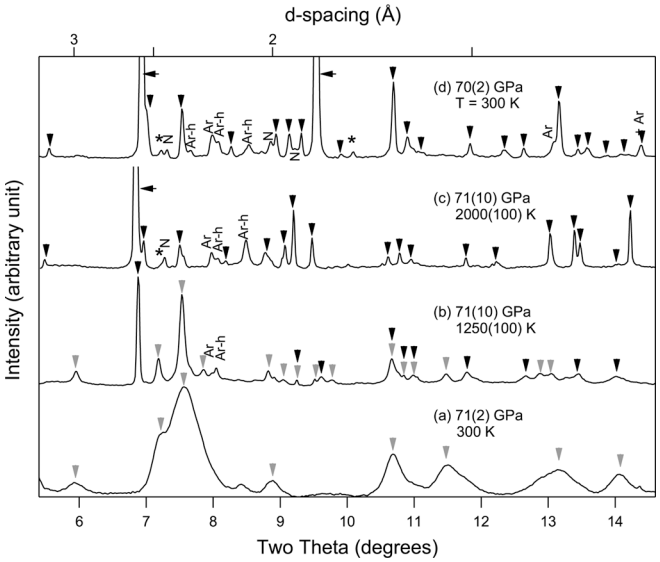

Fig. 2. XRD patterns of the RhII (gray triangles) and PPv-type (black triangles) phases in Fe_2O_3 at high *P*–*T* (X-ray energy = 40 keV; Ar, argon; Ar-hcp, hcp structured Ar; and N, nitrogen; Re, rhenium; ∗, unidentified lines). The backgrounds were subtracted. For the PPv phase in D, we obtained $a = 2.6507(7)$ Å, $b = 8.598(3)$ Å, and $c = 6.413(2)$ Å.

GEOPHYSICS

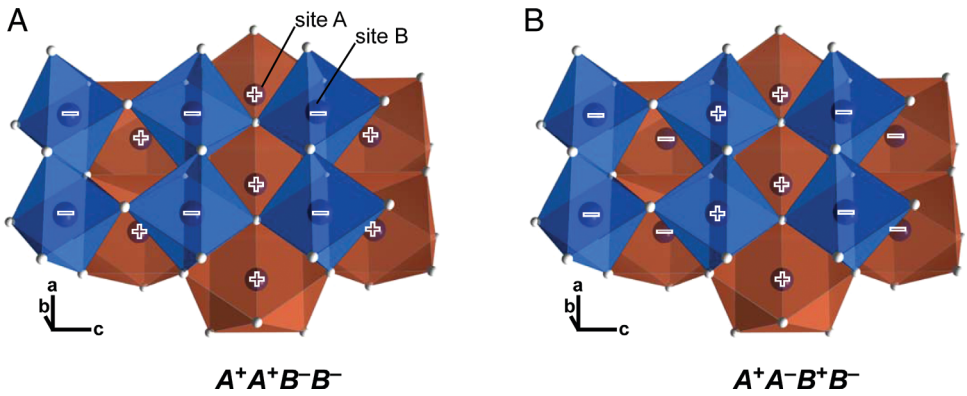

Fig. 3. The spin ordering in the PPv-type Fe_2O_3. The red and blue spheres represent the bipolar-prismatically (site A) and octahedrally (site B) coordinated Fe^{3+} ions, respectively. The gray spheres represent oxygen atoms. The crystallographic orientations of the models are shown at *A* and *B*, *Lower Left*. We denote magnetic arrangements using + and − for up and down moments, respectively.

spin state in Fe_2O_3-PPv, we have conducted ab initio calculations [GGA+U, see supporting information (SI) *Appendix* for calculation details]. We focus on three symmetry distinct collinear HS ferromagnetic (FM) and AFM arrangements in the Fe_2O_3-PPv primitive unit cell, and three corresponding structures with LS on the B site, because we found the A site does not go LS (see below). An additional supercell magnetic arrangement was explored and is discussed in the *SI Appendix*.

First, we consider the two symmetrically distinct AFM arrangements and one FM arrangement in the primitive cell: $A^+A^+B^-B^-$, $A^+A^-B^+B^-$, and $A^+A^+B^+B^+$, where + and − are spin up and down, respectively, and *A* and *B* represent bipolar prismatic and octahedral sites, respectively (Fig. 3). In $A^+A^+B^-B^-$, all Fe atoms in the A site are + and all Fe atoms in the B site are − through AFM interaction along the [111] direction. All spin arrangements along the edge-sharing, [100], and corner-sharing, [001], directions are FM in $A^+A^+B^-B^-$. Arrangement $A^+A^-B^+B^-$ is AFM along [001] and [101] in the B and A sites, respectively, and FM along the edge-sharing direction, [100], in both the A and B sites. These arrangements are modeled with both HS and LS Fe^{3+} on the B site. Because we found no stable LS state on the A site up to 150 GPa, we only consider LS in the B site. Note that the $A^+_{HS}A^+_{HS}B^+_{LS}B^+_{LS}$ (FM) and $A^+_{HS}A^+_{HS}B^-_{LS}B^-_{LS}$ arrangements (the subscripts indicate the spin state of Fe) have a net magnetic moment per primitive cell $12\mu_B$ and $8\mu_B$, respectively. Therefore, the latter arrangement is ferrimagnetic. However, $A^+_{HS}A^-_{HS}B^+_{LS}B^-_{LS}$ has no net magnetic moment, i.e., AFM (see *SI Appendix* for details).

The calculated enthalpies of the different magnetic arrangements and spin states are shown in Fig. 4 for PPv. At low *P*, arrangements with HS Fe^{3+} are more stable than those with LS Fe^{3+} on the B site. Among the HS structures there is a significant gain in stability for AFM over FM arrangements by up to 100 meV per atom. There is no magnetic ordering transition at high *P* if Fe^{3+} remains HS. However, we find the $A^+A^+B^-B^-$, $A^+A^-B^+B^-$, and $A^+A^+B^+B^+$ (FM) arrangements all undergo a *P*-induced spin transition on the B site from HS to LS. For the most stable magnetic arrangement the spin transition occurs at a critical pressure, P_c, of 68 GPa. Below P_c, the most stable magnetic arrangement is $A^+_{HS}A^+_{HS}B^-_{HS}B^-_{HS}$. Above P_c, the most stable arrangement is $A^+_{HS}A^-_{HS}B^+_{LS}B^-_{LS}$. The P_c is very close to the values of 70 GPa where PPv has been measured in SMS work. Because the choice of the Coulomb interaction (U) is somewhat ambiguous and influences P_c (U = 4 eV lowers P_c to 50 GPa and U = 7 eV raises P_c to 110 GPa), we consider both $A^+_{HS}A^+_{HS}B^-_{HS}B^-_{HS}$ and $A^+_{HS}A^-_{HS}B^+_{LS}B^-_{LS}$ magnetic arrangements as candidates for the experimentally observed phase.

The pressure at which the B site Fe^{3+} undergoes a spin transition depends on the magnetic ordering: it occurs at 25 GPa for $A^+A^+B^+B^+$ (FM), at 55 GPa for $A^+A^-B^+B^-$, and at 75 GPa for $A^+A^+B^-B^-$, demonstrating that the AFM arrangements stabilize HS Fe^{3+} on the B site to higher *P*. The spin transition to LS Fe^{3+} on the B site brings $A^+A^+B^-B^-$, $A^+A^-B^+B^-$, and $A^+A^+B^+B^+$ all within 25 meV of each other, suggesting that different magnetic orderings with LS B site are nearly degenerate in energy and all more stable than the same arrangements with HS Fe^{3+} at high pressures. The stable spin arrangements in our ab initio calculations can be also rationalized by considering the crystal structure of PPv combined with superexchange theory (28) (see *SI Appendix*).

In our SMS, the *QS* observed for both sites (−0.31 and 0.48 mm/s) in PPv are consistent with Fe^{3+} ions in the HS state (26). The *QS* of LS Fe^{3+} is expected to be higher than what we observed for PPv (29), as best shown in the high *QS* found in Fe_2O_3-RhII (Table 1), which has all Fe^{3+} in LS according to X-ray emission spectroscopy (21). We obtain small differences in isomer shift, $\Delta IS = 0.30 \pm 0.02$ mm/s, between the two different Fe sites, indicating that the spin and oxidation states of the two Fe sites are likely to be the same (29). From these results and the ab initio calculation, we conclude that the magnetic ordering observed in SMS is likely to be $A^+_{HS}A^+_{HS}B^-_{HS}B^-_{HS}$.

The high B_{hf} of site 1 is also consistent with HS Fe^{3+} (Table 1). However, the B_{hf} of site 2 (19.2 T) is lower than expected

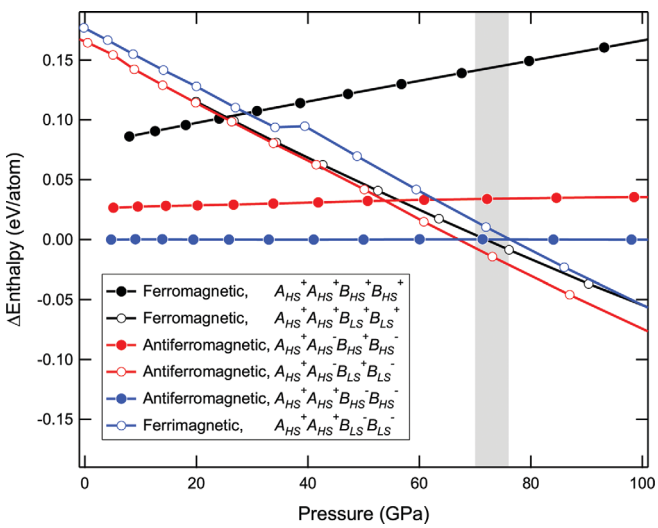

Fig. 4. Stability of different magnetic arrangements and spin states in Fe_2O_3-PPv at high *P*. A reference state consisting of a polynomial fit to the enthalpy of $(A^+_{HS}A^+_{HS}B^-_{HS}B^-_{HS})$, which is the stable state at ambient pressure, is subtracted off each curve. The gray area indicates the *P* where we measured the SMS of PPv. See the text for the notations.

for HS Fe^{3+}. In intermediate spin (IS) and LS states, the moment of Fe^{3+} is expected to reduce to approximately $3\mu_B$ and $1\mu_B$, respectively. Considering that the maximum spin contribution is approximately 11 T per spin for Fe^{3+}, the expected B_{hf} value for the IS and LS states would be 33 and 11 T, respectively, provided that spin contribution is still dominant for B_{hf}. One possibility for the low B_{hf} is the coexistence of different magnetic orderings with different spin states in the PPv phase observed in the experiment. In fact, the ab initio results indicate that at the pressure we measured SMS for PPv the enthalpy differences among $A^+_{HS}A^+_{HS}B^-_{HS}B^-_{HS}$, $A^+_{HS}A^+_{HS}B^-_{LS}B^-_{LS}$, $A^+_{HS}A^-_{HS}B^+_{LS}B^-_{LS}$, and $A^+_{HS}A^+_{HS}B^+_{LS}B^+_{LS}$ are very small. Therefore, if indeed this is the case, the Mössbauer parameters we measured could be averages over some or all of these competing spin arrangements.

In summary, our observations show that magnetism is destroyed and then reconstructed, and the spin state changes from HS to LS and then back to HS (at least for half of Fe^{3+}) during hematite $\rightarrow$ RhII $\rightarrow$ PPv phase transitions. This strong coupling between structural transitions and electronic transitions of Fe has some important planetary and geophysical applications.

Pyrrhotite has been shown to be demagnetized at high P and this has been used for explaining the low magnetic field intensities observed at the impact basins on Mars (16). However, in the case of hematite, our study demonstrates that magnetic ordering can be revived at high P through a structural transition even after complete destruction of the ordering. It remains to be investigated how this sequence of changes would affect the preexisting magnetic records in the carrier mineral. Important questions to be investigated include the critical (Curie or Néel) temperature for Fe_2O_3-PPv and the behaviors of the spin ordering formed in the PPv stability field during fast unloading. Nevertheless, our results highlight that pressure does not necessarily induce demagnetization and the crystal structure of high-P phase can strongly influence the magnetic ordering of the carrier minerals during impacts.

Iron enters mantle phases and plays important roles for the material properties. Recently it has been shown that Fe in mantle silicates and oxides undergoes a HS $\rightarrow$ LS transition (7–9) which influences important physical properties such as density (30), optical properties (11), and electrical conductivity (31). It appears that spin pairing monotonically increases with P in Fp with mantle-related compositions where no significant structural transition exists in the mantle. However, the spin state of Fe in Pv and PPv may be a lot more complicated because of the diverse environments for Fe in those phases (32) and can include spin transition on just a subset of sites (29). Our study on Fe_2O_3 demonstrates that the degree of spin pairing may not increase monotonically with P in the presence of phase transitions in planetary interiors.

Some geodetic observations, nutation, can be explained by a metal-like electrical conductivity in the lowermost part of the mantle (33), which may play an important role for the electromagnetic coupling of the mantle and the core. We explore the electrical conductivity of Fe_2O_3-PPv by using the density of states (DOS) from our ab initio calculation. Arrangement $A^+_{HS}A^+_{HS}B^-_{HS}B^-_{HS}$, which is stable at low P, has a band gap of 0.4 eV. Even with a fixed magnetic moment this gap is small enough that at lower mantle temperatures there will be many thermal electrons for conduction. However, the magnetic coupling is weak enough in the HS phase (FM and AFM have an energy difference of <0.1 eV) that the alloy will likely be paramagnetic (PM) at lower mantle T. Because we found that other HS magnetic structures have no gap (e.g., $A^+_{HS}A^-_{HS}B^+_{HS}B^-_{HS}$ and $A^+_{HS}A^+_{HS}B^+_{HS}B^+_{HS}$), we expect that the HS PM phase will be metallic. All the phases with LS Fe^{3+} on the B site will be PM under lower mantle conditions, since the magnetic coupling is very weak in the LS state. The DOS for $A^+_{HS}A^+_{HS}B^-_{LS}B^-_{LS}$, $A^+_{HS}A^-_{HS}B^+_{LS}B^-_{LS}$, and $A^+_{HS}A^+_{HS}B^+_{LS}B^+_{LS}$ all show metallic behaviors suggesting that the LS PM alloy will be metallic as well.

To further verify that the high-P PM state is metallic, we directly calculated an approximate PM unit cell by using the special quasi-random structure (SQS) approach (34). The DOS for the two SQS were found at 40 GPa with $A_{HS}A_{HS}B_{HS}B_{HS}$ and 70 GPa with $A_{HS}A_{HS}B_{LS}B_{LS}$. The DOS of the disordered magnetic arrangements in both SQS structures at both pressures show no gap and are therefore metallic. This further supports the claim of a metallic PM alloy. Therefore, we predict metallic behavior for Fe_2O_3-PPv under lower mantle P–T conditions. This result is qualitative as no attempt has been made to determine the electron or hole mobility and the possible effects of defects and impurities have not been included.

A large drop in electrical resistivity to a level of a semiconductor has been documented in Fe_2O_3-RhII (17–19). Combined with our findings from ab initio calculations, this indicates that the electrical conductivity of Fe_2O_3 is further enhanced to that of a metal at the RhII $\rightarrow$ PPv transition.

Recently, it has been reported that $(Mg_{0.9}Fe_{0.1})SiO_3$-PPv has a large electrical conductivity and proposed that a 200-km-thick layer of $(Mg_{0.9}Fe_{0.1})SiO_3$-PPv, i.e., the D″ layer, would explain the geodetic observations (35). Yet it is important to know how Fe is distributed among the phases because Fe concentration is critical for the electrical conductivity. A study on a pyrolitic composition showed that Fe^{2+} preferentially enters Fp and is <3 mol% in mantle PPv (36), whereas another study on an olivine composition proposed the opposite (37). If the former is the case, then the electrical conductivity of mantle PPv should be very low and may not be important for the electromagnetic coupling. Furthermore, even with the Fe enrichment, the electrical conductivity of Fp remains quite low at high P and the Fe spin transition at midmantle P further decreases the conductivity (31).

An alternative possibility is local enrichment of Fe at the core-mantle boundary (CMB). It has been proposed that the ultra-low-velocity zones observed seismologically at the CMB (38) can be explained by Fe-enriched PPv (39). Furthermore, recent studies have shown enhancement in the concentration of Fe^{3+} by Al in both mantle Pv and PPv (22, 23). It is notable that the basaltic layer at the top of the subducting slab has a high concentration of Al and some seismic studies have suggested that the subducting slabs reach CMB (40). In addition, the basaltic layers become negatively buoyant in the lower mantle (41) and likely are transported to the CMB. Therefore, possible accumulation of basaltic materials at the CMB is also a candidate for the high electrical conductivity at the CMB, as Fe^{3+}–O bonding becomes metallic at deep mantle P as found in this study. Also, an enhanced Fe^{3+}/Fe^{2+} ratio would increase the electrical conductivity through electron hopping between these two species (42).

Methods

Pure $^{57}Fe_2O_3$ was loaded in the diamond-anvil cell with 2–3 ruby chips for P measurements. Argon was loaded as a pressure-transmitting and insulation medium. We conducted SMS and XRD at Advanced Photon Source (APS). For SMS, X-rays with bandwidths of 1 meV were tuned to the nuclear transition energy of ^{57}Fe. The time spectra were obtained by using an avalanche photodiode detector. Angle-dispersive diffraction was conducted in the double-sided laser-heated diamond cell by using a monochromatic X-ray beam.

Calculations were performed with the Vienna Ab-initio Simulation Package (VASP), using density functional theory (DFT) and the projector-augmented plane-wave (PAW) method. Exchange correlation was treated in the Perdew–Burke–Ernzerhof (PBE) Generalized Gradient Approximation (GGA) by using a soft oxygen pseudopotential. The Brillouin zone was sampled by a Monkhorst–Pack k-point mesh of $7\times7\times4$ for the primitive 10-atom unit cell. Energy convergence with respect to k-points was better than 1 meV per atom. A U value of 5 eV ($J = 1$ eV) is used to obtain the correct ground-state properties. The Fe-substituted PPv structure is fully relaxed at ambient P and then a series of fixed volume calculations, each internally relaxed, are performed to explore stability as a function of P. For high P PM state, we calculated an approximate PM unit cell by using the SQS approach (see *SI Appendix* for details and references).

ACKNOWLEDGMENTS. We thank B. Weiss and T. L. Grove for discussions that improved this article and the editor and two anonymous reviewers for helpful comments and suggestions. This work was supported by the National Science Foundation (NSF) Grants EAR0738655 (to S.H.S.) and EAR0738886 (to D.M.), respectively. K.C. is supported by a Departmentof Energy (DOE) National Nuclear Security Administration Stewardship Science Graduate Fellowship. Measurements were performed at Sectors 3 and GeoSoilEnviroCars (GSECARS) at Advanced Photon Source. GSECARS is supported by the NSF and DOE. Use of Sector 3 was supported in part bythe Consortium for Materials Properties Research in Earth Sciences under NSF Cooperative Agreement EAR 06-49658. Use of the APS was supported by the DOE, Office of Science, Office of Basic Energy Sciences, under Contract No. DE-AC02-06CH11357.

1. Ono S, Ohishi Y (2005) In situ x-ray observation of phase transformation in Fe_2O_3 at high pressures and high temperatures. *J Phys Chem Solids* 66:1714–1720.
2. Murakami M, Hirose K, Kawamura K, Sata N, Ohishi Y (2004) Post-perovskite phase transition in $MgSiO_3$. *Science* 304:855–858.
3. Oganov AR, Ono S (2004) Theoretical and experimental evidence for a post-perovskite phase of $MgSiO_3$ in Earth's D″ layer. *Nature* 430:445–448.
4. Shim SH, Duffy TS, Jeanloz R, Shen G (2004) Stability and crystal structure of $MgSiO_3$ perovskite to the core-mantle boundary. *Geophys Res Lett* 31:L10603.
5. Knittle E, Jeanloz R (1986) High-pressure metallization of FeO and implications for the Earth's core. *Geophys Res Lett* 13:1541–1544.
6. Cohen RE, Mazin II, Isaak DG (1997) Magnetic collapse in transition metal oxides at high pressure: Implications for the Earth. *Science* 275:654–657.
7. Badro J, et al. (2003) Iron partitioning in Earth's mantle: Toward a deep lower mantle discontinuity. *Science* 300:789–791.
8. Badro J, et al. (2004) Electronic transitions in perovskite: Possible nonconvecting layers in the lower mantle. *Science* 305:383–386.
9. Li J, et al. (2004) Electronic spin state of iron in lower mantle perovskite. *Proc Natl Acad Sci USA* 101:14027–14030.
10. Lin JF, et al. (2005) Spin transition of iron in magnesiowüstite in the Earth's lower mantle. *Nature* 436:377–380.
11. Goncharov AF, Stuzhkin VV, Jacobsen SD (2006) Reduced radiative conductivity of low-spin (Mg,Fe)O in the lower mantle. *Science* 312:1205–1208.
12. Persson K, Bengtson A, Ceder G, Morgan D (2006) Ab initio study of the composition dependence of the pressure-induced spin transition in the $(Mg_{1-x}Fe_x)O$ system. *Geophys Res Lett* 33:L16306.
13. Bengtson A, Persson K, Morgan D (2007) Ab initio study of the composition dependence of the pressure-induced spin crossover in perovskite $(Mg_{1-x}Fe_x)SiO_3$. *Earth Planet Sci Lett* 265:535–545.
14. Crawford DA, Schultz PH (1988) Laboratory obaservations of impact-generated magnetic fields. *Nature* 336:50–52.
15. Carporzen L, Gilder SA, Hart RJ (2005) Palaeomagnetism of the Vredefort meteorite crater and implications for craters on Mars. *Nature* 435:198–201.
16. Rochette P, et al. (2003) High pressure magnetic transition in pyrrhotite and impact demagnetization on Mars. *Geophys Res Lett* 30:1683.
17. Kondo K, Mashimo T, Sawaoka A (1980) Electrical resistivity and phase transformation of hematite under shock compression. *J Geophys Res* 85:977–982.
18. Knittle E, Jeanloz R (1986) High-pressure electrical resistivity measurements of Fe_2O_3: Comparison of static-compression and shock-wave experiments to 61 GPa. *Solid State Commun* 58:129–131.
19. Pasternak MP, et al. (1999) Breakdown of the Mott-Hubbard state in Fe_2O_3: A first-order insulator-metal transition with collapse of magnetism at 50 GPa. *Phys Rev Lett* 82:4663–4666.
20. Olsen JS, Cousins CSG, Gerward L, Jhans H, Sheldon BJ (1991) A study of the crystal structure of Fe_2O_3 in the pressure range up to 65 GPa using synchrotron radiation. *Phys Scr* 43:327–330.
21. Badro J, et al. (2002) Nature of the high-pressure transition in Fe_2O_3 hematite. *Phys Rev Lett* 89:205504.
22. McCammon C (1997) Perovskite as a possible sink for ferric iron in the lower mantle. *Nature* 387:694–696.
23. Sinmyo R, Hirose K, O'Neill HSC, Okunishi E (2006) Ferric iron in Al-bearing post-perovskite. *Geophys Res Lett* 33:L12S13.
24. Bruzzone CL, Ingalls R (1983) Mössbauer-effect study of the Morin transition and atomic positions in hematite under pressure. *Phys Rev B* 28:2430–2440.
25. Suzuki T, et al. (1985) *Solid State Physics under Pressure*, ed Minomura S (Terra Scientific Publishing Company, Tokyo, Japan), pp. 149–154.
26. Hawthorne FC, ed (1988) *Spectroscopic Methods in Mineralogy and Geology*, Reviews in Mineralogy (Mineralogical Society of America, Chantilly, VA), vol 18.
27. Shim SH, et al. (2008) Crystal structure and thermoelastic properties of $(Mg_{0.91}Fe_{0.09})SiO_3$ postperovskite up to 135 GPa and 2700 K. *Proc Natl Acad Sci USA* 105:7382–7386.
28. Goodenough JB (1963) *Magnetism and the Chemical Bond* (Interscience Publishers, New York).
29. Jackson JM, et al. (2005) A synchrotron Mössbauer spectroscopy study of $(Mg,Fe)SiO_3$ perovskite up to 120 GPa. *Am Mineral* 90:199–205.
30. Fei Y, et al. (2007) Spin transition and equation of state of (Mg,Fe)O solid solution. *Geophys Res Lett* 34:L17307.
31. Lin JF, et al. (2007) Electrical conductivity of the lower-mantle ferropericlase across the electron spin transition. *Geophys Res Lett* 34:L16305.
32. Lundin S, et al. (2008) Effect of Fe on the equation of state of mantle silicate perovskite over 1 Mbar. *Phys Earth Planet Inter* 168:97–102.
33. Buffett BA, Garnero EJ, Jeanloz R (2000) Sediments at the top of Earth's core. *Science* 290:1338–1342.
34. Wei SH, Ferreira LG, Bernard JE, Zunger A (1990) Electronic properties of random alloys: Special quasirandom structures. *Phys Rev B* 42:9622–9649.
35. Ohta K, et al. (2008) The electrical conductivity of post-perovskite in Earth's D″ layer. *Science* 320:89–91.
36. Murakami M, Hirose K, Sata N, Ohishi Y (2005) Post-perovskite phase transition and mineral chemistry in the pyrolitic lowermost mantle. *Geophys Res Lett* 32:L03304.
37. Kobayashi Y, et al. (2005) Fe-Mg partitioning between $(Mg,Fe)SiO_3$ post-perovskite, perovskite, and magnesiowüstite in the Earth's lower mantle. *Geophys Res Lett* 32:L19301.
38. Revenaugh J, Meyer R (1997) Seismic evidence of partial melt within a possibly ubiquitous low-velocity layer at the base of the mantle. *Science* 277:670–673.
39. Mao WL, et al. (2006) Iron-rich post-perovskite and the origin of ultralow-velocity zones. *Science* 312:564–565.
40. van der Hilst RD, Widiyantoro S, Engdahl ER (1997) Evidence for deep mantle circulation from global tomography. *Nature* 386:578–584.
41. Hirose K, Fei Y, Ma YZ, Mao HK (1999) The fate of subducted basaltic crust in the Earth's lower mantle. *Nature* 397:53–56.
42. Shankland TJ, Peyronneau J, Poirier JP (1993) Electrical conductivity of the Earth's lower mantle. *Nature* 366:453–455.